Resonance and intermediate-coupling effects in electron scattering with highly charged ions. II. Autoionization and dielectronic recombination

A. K. Pradhan*
Department of Physics, University of Windsor, Windsor, Ontario N9B 3P4, Canada
(Received 15 April 1983)

The role of resonances in electron-impact excitation of highly charged ions is examined and some methods are described in order to take account of autoionization and dielectronic recombination. The intermediate-coupling calculations of paper I are extended to include these processes and effective collision strengths are obtained. Results are presented to illustrate particular features in a number of transitions in Fe^{24+} and Mo^{40+}. Resonance analysis is carried out employing numerical interpolation techniques and multichannel quantum-defect theory, employing reactance matrices in nine-state close-coupling and distorted-wave approximations. It is shown that all three effects considered in the present study, departure from *LS* coupling, resonance enhancement due to autoionization, and reduction in autoionization enhancement due to dielectronic recombination, can be of considerable importance in the cross sections of highly ionized systems. In the high-Z ions of the helium isoelectronic sequence the contribution of autoionizing resonances remains large even after all probable radiative channels are included, although the net autoionization effect decreases with Z.

I. INTRODUCTION

In an important paper, VIIth in the series of papers on the quantum-defect theory, Seaton[1] extended the multichannel quantum-defect theory (MCQDT) to the analysis of resonances in electron-ion scattering cross sections. The theory given also included a description of the formulation due to Gailitis[2] for analytic integration over Rydberg series of poles in the scattering matrix, corresponding to series of resonances below the threshold, or thresholds, of convergence, leading to an expression for the resonance averaged cross section. Seaton also showed that, in the limit of large Z, the resonances approach a δ-function form, the integration over which yields a contribution of the *same order* as the nonresonant contribution. Thus, we expect that the ratio of the resonant to nonresonant parts of the cross section, i.e., resonance enhancement *relative* to the background, should approach a constant. The study of resonance effects along an isoelectronic sequence, by Pradhan, Norcross, and Hummer (PNH, Ref. 4 of paper I) and the present one, indicates exactly such a pattern as similar factors of resonance enhancement are obtained for a given transition along the helium sequence. However, resonances arising from autoionizing states embedded in the continuum are not the only process to consider when the cross sections of highly charged ions are concerned. It was shown by Presnyakov and Urnov[3] that for multiply charged ions the autoionization (AI) effect would be mitigated by the onset of radiative decay of the resonance states as the radiative probability increases as Z^4 (only allowed transitions are considered for the moment; other types of transitions are also discussed later). Therefore, whenever the radiative probabilities begin to compete with AI, the dielectronic recombination (DER) process would occur and its effect on the total cross section should be taken into account. Employing the MCQDT and the formulation by Presnyakov and Urnov, Pradhan[4] calculated the effect of DER in reducing AI relative to the background cross sections, for O^{6+} and $Fe^{24}+$. These calculations were, however, carried out in *LS* coupling which, as discussed in paper I, is not valid for a number of transitions in highly charged He-like ions. Therefore, the AI and the DER effects must be considered in an IC scheme. The computational procedure by Saraph[5] has now been extended to incorporate all three processes.[6] In the present work we investigate the net effect on the collision strengths and compute final effective values, taking account of detailed resonance structures.

II. THEORY

Numerical and analytical techniques based on the general theory of resonances and MCQDT are employed in order to analyze completely the resonances present in multichannel electron-ion scattering. The asymptotic behavior of the radial wave functions of the scattering electron [Eq. (1b) of paper I] may be expressed in terms of the reactance matrices $\underline{R}$ as

$$\underline{R} \underset{\rightarrow}{\sim}_{\infty} k^{-1/2}[(\sin\xi)\mathbb{1}+(\cos\xi)\underline{R}] , \tag{1}$$

where ξ is the regular Coulomb phase (k and ξ are diagonal). The $\underline{R}$ matrices have the advantage of being real as opposed to the scattering matrices S which are complex. As the zeros of the Jost function in the complex p plane are simple, in the vicinity of an isolated resonance we may write the $\underline{S}$ matrix as

$$\underline{S}=\mathbb{1}-\frac{i\underline{C}}{(E-E_0+i\Gamma/2)} , \tag{2}$$

where the pole position is $E_0-i\Gamma/2$; E_0 lies on the real axis and Γ (>0) is the deviation along the imaginary axis

(resonances correspond to the poles in the lower half of the second Riemann sheet in the E plane. It may be shown that the residue matrix $\underline{C}$ ($C^2=\Gamma C$) is Hermitian and that its elements may be factorized as

$$C_{ij}=\pm c_i c_j \ , \tag{3}$$

(only the positive sign may be retained). Since

$$\underline{R}=i(\mathbf{1}-\underline{S})(\mathbf{1}+\underline{S})^{-1} \ , \tag{4}$$

close to the resonance we obtain

$$\underline{R}=\underline{R}^{bg}-\frac{\underline{C}}{(E-E_0)} \ , \tag{5}$$

where $\underline{R}^{bg}$ is a slowly varying background term that may be expressed by a polynomial in energy. Finally, using (3) the individual elements may be written as

$$R_{ij}(\epsilon)=\sum_k a_k \epsilon^{k-1}+\sum_l \frac{c_i c_j}{(E-E_l)} \ , \tag{6}$$

where c_i, c_j are factors of residue at pole energy E_l. Comparing Eqs. (5) and (6) it is seen that the product $c_i c_j$ must now be *negative.*

In the region of some closed channels, one may make an analytic continuation of the $\underline{R}$ matrix which may then be partitioned as

$$\underline{\mathscr{R}}=\begin{bmatrix} \underline{\mathscr{R}}_{oo} & \underline{\mathscr{R}}_{oc} \\ \underline{\mathscr{R}}_{co} & \underline{\mathscr{R}}_{cc} \end{bmatrix} \ , \tag{7}$$

where $\underline{\mathscr{R}}$ is the analytic continuation and *oo* refers to open-open, *oc* to open-closed, etc. Seaton has derived (Ref. 1), in the region below threshold with resonances, the $\underline{R}$ matrix to be given by

$$\underline{R}=\underline{\mathscr{R}}_{oo}-\underline{\mathscr{R}}_{oc}[\tan(\pi\nu_c)\mathbb{1}+\underline{\mathscr{R}}_{cc}]^{-1}\underline{\mathscr{R}}_{co} \ , \tag{8}$$

where ν_c is the effective quantum number in the closed channels. Eisner and Seaton[7] make a first-order Taylor expansion in (8) about the resonance energy $E^{(0)}$ and thereby obtain the same expression, Eq. (6), for numerical interpolation in the resonance region. Resonance profiles for a complete Rydberg series may now be obtained.

In the region below threshold, Gailits (Ref. 2) has shown that the resonance averaged $\underline{S}$ matrix is given by (see also Ref. 1)

$$\langle |S_{ij}|^2\rangle = |\chi_{ij}|^2+\sum_{n,m}\frac{\chi_{in}\chi_{nj}\chi^*_{im}\chi^*_{mj}}{1-\chi_{nn}\chi^*_{nm}} \ , \tag{9}$$

where the matrix $\underline{\chi}=\underline{S}=(i\mathbb{1}-\underline{R})(i\mathbb{1}+\underline{R})^{-1}$ for all channels open and may be partitioned as in Eq. (7) in the region of some open channels and some closed (indices i,j refer to open and n,m refer to closed channels). Equation (9) may be simplified as

$$\langle |S_{ij}|^2\rangle = |\chi_{ij}|^2+\sum_{n=1}^{M}\frac{|\chi_{in}|^2|\chi_{nj}|^2}{\sum_k |\chi_{nk}|^2} + 2\,\mathrm{Re}\sum_{\substack{n,m \\ n\neq m}}\left[\frac{\chi_{in}\chi_{nj}\chi^*_{im}\chi^*_{mj}}{1-\chi^*_{nn}\chi^*_{mm}}\right] . \tag{10}$$

Equations (9) and (10) are derived after diagonalizing the submatrix $\underline{\chi}_{cc}$ and making use of the unitarity of the $\underline{S}$ matrix, i.e.,

$$1-|\chi_{nn}|^2=\sum_k |\chi_{nk}|^2 \ ,$$

where k refers to all remaining open channels in the region below threshold. The sum in Eq. (10) extends over all M closed channels and represents the probability of capture $|\chi_{in}|^2$ into a resonance state, corresponding to closed channel n, and the probability of subsequent decay through autoionization,

$$\frac{|\chi_{nj}|^2}{\sum_k |\chi_{nk}|^2} \ ,$$

into open channel j. The third term in Eq. (10) represents interference effects between closed channels and is usually small, particularly for highly charged ions. In Ref. 4 Eq. (10) has been modified to include the branching between autoionization and radiative decay, and the role of DER in the scattering process is investigated in the *LS* coupling scheme. In the present work we transform the $\underline{R}$ matrices to a pair-coupling scheme as described in paper I (Sec. II) and the $\underline{\chi}$ matrices in IC are computed. Equation (10) may now be written as

$$\langle |S_{ij}|^2\rangle_d = |\chi_{ij}|^2+\sum_{n}^{M}\frac{|\chi_{in}|^2|\chi_{nj}|^2}{\left[\sum_k |\chi_{nk}|^2+\sum_b\left[\frac{2\pi\nu^3}{z^2}\right]\Gamma_{nb}(S_nL_nJ_n\rightarrow S_bL_bJ_b)\right]} + 2\,\mathrm{Re}\left[\sum_{\substack{n,m \\ n\neq m}}\frac{\chi_{in}\chi_{nj}\chi^*_{im}\chi^*_{mj}}{1-\chi^*_{nn}\chi^*_{mm}}\right] . \tag{11}$$

In Eq. (11) the sum over the radiative probabilities Γ_{nb} is for all transitions that may occur between the core states associated with the closed resonance channel n and the bound *or* quasibound channel b. In other words, we include (and later show) that in addition to "primary" DER, i.e., direct recombination to the ground state of the recombining ion, transitions may also take place between resonance channels associated with different core states, provided the radiative transition probability is sufficiently competitive with autoionization *and* the primary mode of stabilization. We refer to the latter process as "secondary" DER and the implication is that in scattering with highly charged ions involving excited complexes, final stabilization of the recombining electron would involve a ra-

diative cascade mechanism via a series of autoionizing states belonging to core states of different complexes. The spectator electron is assumed to have the same quantum numbers nlj throughout the recombining process. If we assume the analytic continuation of the $\underline{S}$ matrix below threshold to be constant, then the energy variation of the averaged DER contribution (or the averaged DER cross section; see Ref. 4), results from the $1/\nu^3$ decrease of the autoionization probabilities along the Rydberg series.

The second term on the right-hand side (rhs) of Eq. (11) may be further subdivided if we consider the fact that nondipole core transitions have small decay probabilities compared to dipole transitions. Then we write the second term as

$$\sum_{n'} \frac{|\chi_{in'}|^2 |\chi_{n'\beta}|^2}{\sum_k |\chi_{n'k}|^2 + \sum_b \Gamma_D(S_n L_n I_n, S_b L_b J_b)} + \sum_{\substack{m=1 \\ m\neq n'}}^{M} \frac{|\chi_{im}|^2 |\chi_{mj}|^2}{\sum_k |\chi_{mk}|^2},$$

where n' indicates the sum over closed channels with available dipole transitions $n' \rightarrow b$. If the radiative probability Γ_D is much higher than the autoionization probability, the first sum may become very small and the remaining resonance enhancement in the cross section would result from the second sum, i.e., through closed channels m that do not have an associated dipole core transition to lower states.

III. CALCULATIONS

In the present approximation including nine LS states in the eigenfunction expansion, resonances are present in the cross sections for transitions involving the $n=2$ states. The energy region of interest is from the excitation threshold to the $n=3$ levels. Some resonance structures are present in the region in between the various $n=2$ states; however, this range is too small to be of practical consequence (LS coupling resonance calculations for Fe^{24+} have been carried out by PNH in this region). The dominant resonance contribution comes from the large energy range between the $n=2$ and the $n=3$ levels and it is here that we analyze the resonance structures in detail. Nine-state cc calculations were done for Fe^{24+}, $l \leq 4$, at a few energies above the $n=3$ states. All other calculations are in a nine-state DW approximation.

The MCQDT analysis of resonances sketched in Sec. II would not yield the structure due to the lowest group of resonances corresponding to equivalent (not Rydberg) electron orbitals, e.g., $1s3l^2$. Therefore, the calculations are divided into two parts: (i) direct computations of IC collision strengths at a large number of energies in the range covered by the $1s3l3l'$ group of resonances and (ii) MCQDT calculations for the detailed resonance structure, and averaged contributions, in the remainder of the region up to the $n=3$ levels. Following is a brief description.

A. $1s3l3l'$ group of resonances

PNH (see their Table IV) have calculated the positions of these resonances from an atomic structure calculation for the bound states of the (e plus ion) system [Eq. (3) of paper I]. LS coupling calculations are first carried out for Fe^{24+} to obtain $\underline{R}^{LS}$ at a number of energies from 500 to 515 Ry. The lowest $1s3l3l'$ type resonance is $1s3s^2$ at 506.26 Ry and the highest is $1s3d^2$ at 511.32 Ry. Altogether there are 12 such resonances in this group. The $\underline{R}^{LS}$ for all symmetries $SL\pi$ arising from $l,l' \leq 4$ are then transformed to pair-coupling and IC collision strengths are obtained as described in paper I. Resonances corresponding to $l>4$ are not considered in this work as these belong to $n>5$ and therefore lie close to the threshold of convergence. In fact, there are within the last one fifth of the energy difference ΔE_n between the $n=2$ and the $n=3$ complexes and, as shall be seen later, these high-n resonances would largely undergo radiative decay and not enhance the excitation cross section significantly. The $\underline{R}^{LS}$ for the total $SL\pi$ states corresponding to resonances are numerically interpolated using the fitting form given by Eq. (6) and the parameters of fit, a_k, c_i, and E_l, are determined. Transformation from LS coupling to IC implies that the resonance structures in the IC collision strengths correspond to the total $J\pi$ continua (e.g., to the closed channels of Table III in paper I); although we do not explicitly label the fine structure of the individual resonances.

B. Rydberg resonances

For resonances $1s3lnl'$ ($n>3$) we employ MCQDT for computing both the detailed profiles and the resonance averaged collision strengths. The individual $\underline{S}$ matrix elements below threshold are given by (Martins and Seaton[8])

$$S_{ij}(\nu) = \chi_{ij} - \sum_n \chi_{in}(\chi_{nn} - e^{-2\pi i \nu_n})^{-1} \chi_{n\beta}, \tag{12}$$

where the $\underline{\chi}$ matrix elements are the analytic continuation from above threshold. The energy E is expressed in terms of the variable effective quantum number $\nu(E) = z/(E_n - E)^{1/2}$, where E_n is the threshold of convergence. In the present calculations the structures due to the group of resonances labeled $1s3l4l'$ are computed from Eq. (12).

The Gailitis averaged collision strengths $\langle \Omega \rangle$ are computed at a few energies in the region of resonances. The averaged values are slowly varying with energy. The effect of DER is taken into account by including in Eq. (11) the radiative decay probabilities of the transitions between the $n=3$ core states, associated with the closed channels, and the ground state and the $n=2$ states. We need only consider optically allowed radiative transitions as the DER through forbidden core transitions is found to be negligible for the ions considered here (discussed later). In Tables I and II we give the decay rates for all possible dipole transitions from the $n=3$ levels for Fe^{24+} and Mo^{40+}, respectively. Calculations are carried out for the detailed and the averaged collision strengths (with DER) for all transitions involving the $n=2$ states. In Sec. IV a

TABLE I. Radiative probabilities for DER with Fe^{24+}.

$3^3S_1 \rightarrow 2^3P_0(2.54\times10^{11})$, $2^3P_1(8.70\times10^{11})$,[a] $2^3P_2(1.50\times10^{12})$, $2^1P_1(7.89\times10^{10})$
$3^3P_0 \rightarrow 2^3S_1(8.43\times10^{12})$, $3^3S_1(3.44\times10^{7})$
$3^3P_1 \rightarrow 1^1S_0(1.50\times10^{13})$,[a] $2^1S_0(7.22\times10^{11})$, $2^3S_1(8.08\times10^{12})$,[a] $3^3S_1(4.65\times10^{7})$, $3^1S_0(138\times10^{3})$
$3^3P_2 \rightarrow 2^3S_1(8.29\times10^{12})$, $3^3S_1(1.80\times10^{8})$
$3^1S_0 \rightarrow 2^3P_1(1.56\times10^{11})$, $2^1P_1(2.50\times10^{12})$[a]
$3^1P_1 \rightarrow 1^1S_0(1.24\times10^{14})$,[a] $2^1S_0(7.75\times10^{12})$,[a] $2^3S_1(6.78\times10^{11})$, $3^3S_1(4.02\times10^{7})$, $3^1S_0(7.80\times10^{7})$

[a]Wiese (private communication). All radiative rates are in s^{-1}.

few selected results are presented in order to illustrate the method and the general pattern of the net effective collision strengths.

IV. RESULTS AND DISCUSSION

Forbidden transitions often have large AI enhancements. We study two such transitions, 1^1S_0-2^3S_1 and 2^3S_1-2^1S_0, and determine precisely the effect of AI and DER reduction in each. Figure 1(a) shows the extensive resonance structure present in the former transition in the energy range from threshold to the $n=3$ complex. The two groups of resonances $1s3l3l'$ and $1s3l4l'$ are clearly separated and have similar form except for the very first resonance in each group. In the $1s3l3l'$ group this is a strong resonance associated with the $1s3s^2(^2S,J=\frac{1}{2})$ autoionizing state, while in the $1s3l4l'$ group it is no longer the case. Also, the AI widths in the latter group are significantly narrower. There are some discrepancies in the details of the resonances due mainly to numerical causes; however, the main pattern is clear and would be repeated each time n is incremented by unity (note the breaks in the energy scale indicating further that each n group is well isolated). The dashed line is the Gailitis averaged collision strength. As expected, it is nearly constant over the entire energy range under consideration. The straight solid line above the energy of the $n=3$ states (considered degenerate) is the nonresonant collision strength as given in Table IV of paper I. In Fig. 1(b) we plot again the averaged $\langle\Omega\rangle$ (dashed line) and the averaged $\langle\Omega\rangle$ allowing for radiative decay. The DER contribution is given by the difference between the dashed line and the bottom-most solid line marked 6. The solid lines lying in between reflect the contributions due to the individual $n=3$ states, e.g., the line marked 1 is the effective $\langle\Omega\rangle$ if only the resonances converging on to the first $n=3$ state, 3^3S_1, are allowed to undergo radiative decay; line 2 corresponds to 3^3S_1 *and* 3^3P_0, line 3 to 3^3S_1, 3^3P_0, and 3^3P_1, and so on until line 6 which means that resonances due to all six $n=3$ states may radiate. The area enclosed between line 0 (no radiative decay, i.e., Gailitis $\langle\Omega\rangle$) and line 6 is slightly greater than one tenth of the total area under the dashed line and the background cross section (the solid line from above the $n=3$ states extrapolated backwards). Thus, about one tenth of the electron flux trapped in the AI states goes into DER and the effective cross section is reduced by this amount. However, the reduction in the rate coefficient due to DER would be less than 10% since the cross section at lower energies, where the DER reduction is small, contributes more to the rate (cross section times $e^{-E/kT}$) than the cross section at higher energies that is more susceptible to DER reduction. The AI probabilities decrease as $1/n^3$ and are dominated by radiative decay particularly in the region just below the $n=3$ thresholds. The fact that the net effective collision strength after taking account of AI and DER joins exactly with the nonresonant collision strength at the $n=3$ threshold implies that the DER contribution, through the dipole transitions included (Table I) is equal to the flux in the newly open channels. If DER through the forbidden core transitions were also to be significant then we should expect a larger decrease in the effective cross section throughout the range under consideration. However, even at $Z=42$ the forbidden transitions are a few orders of magnitude less probable than the allowed ones.

In Fig. 1(c) we consider radiative decay of the resonances through core transitions directly to the ground state, i.e., $S_iL_iJ_i\ nlj \rightarrow 1^1S_0\ nlj$. The solid line is the effective collision strength after such decays and it is seen that DER to the ground state through a direct primary core transition turns out to be a small component of the total. Only the resonance series $3^1P_1\ nlj$ and $3^3P_1\ nlj$ have sufficiently large radiative probabilities of doing so (see Table I). For these AI states the fractional decay is ~1.0 and ~0.6, respectively, i.e., almost all of the $3^1P_1\ nlj$ and about 60% of the $3^3P_1\ nlj$ resonances decay directly to the ground state and stabilize. Resonances converging on to other $n=3$ states decay preferentially to the $n=2$ states

TABLE II. Radiative probabilities for DER with Mo^{40+}.

$3^3S_1 \rightarrow 2^3P_0(1.41\times10^{12})$, $2^3P_1(3.39\times10^{12})$, $2^3P_2(1.12\times10^{13})$, $2^1P_1(1.67\times10^{12})$
$3^3P_0 \rightarrow 2^3S_1(5.93\times10^{13})$, $3^3S_1(6.20\times10^{7})$
$3^3P_1 \rightarrow 1^1S_0(1.67\times10^{14})$, $2^3S_1(4.52\times10^{13})$, $2^1S_0(1.44\times10^{13})$, $3^3S_1(8.24\times10^{7})$, $3^1S_0(8.24\times10^{2})$
$3^3P_2 \rightarrow 2^3S_1(5.68\times10^{13})$, $3^3S_1(3.94\times10^{9})$
$3^1S_0 \rightarrow 2^3P_1(2.57\times10^{12})$, $2^1P_1(1.51\times10^{13})$
$3^1P_1 \rightarrow 1^1S_0(6.12\times10^{14})$, $2^3S_1(1.33\times10^{13})$, $2^1S_0(4.43\times10^{13})$, $3^3S_1(1.39\times10^{9})$, $3^1S_0(1.85\times10^{9})$

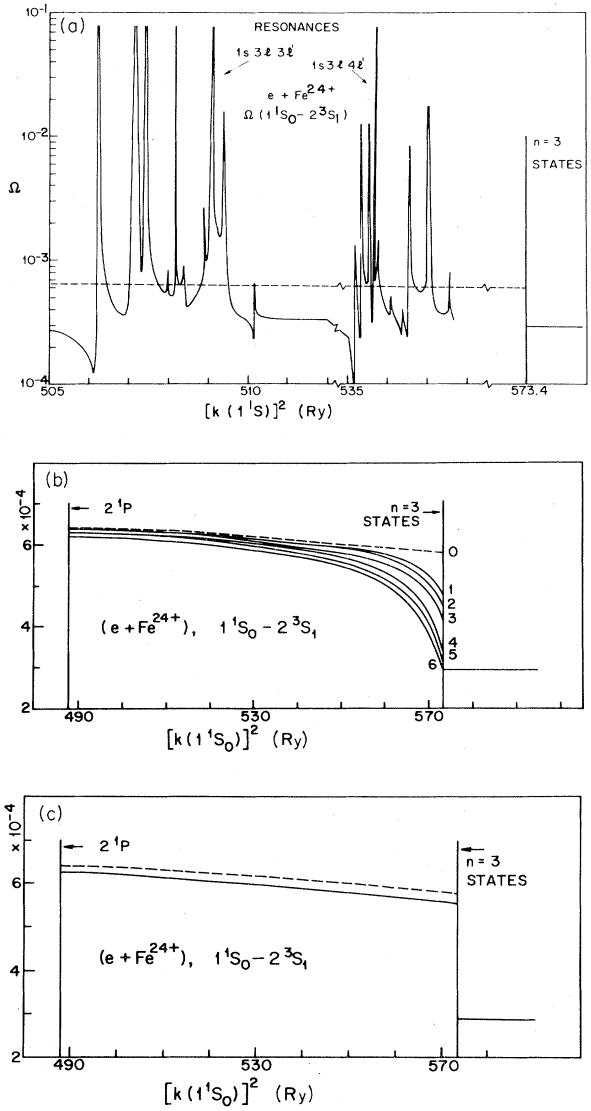

FIG. 1. Collision strength for the transition 1^1S_0-2^3S_1: (a) resonance structures between the $n=2$ and the $n=3$ complexes. Dashed line indicates the Gailitis average (approximately twice the nonresonant value above the $n=3$ threshold. (b) collision strength averaged over autoionizing resonances (dashed line), including the effect of DER (solid lines; see text). (c) Averaged collisions strength with DER directly to the ground state (solid line).

via allowed core transitions and thus most of the recombined electron flux would appear in the form of high-n unresolved satellites of the $n=2$ lines. For example, the primary recombination for the $3^3S_1\,nlj$ series would be largely through the transitions $3^3S_1 \rightarrow 2^3P_{J_i}\,nlj$ ($J_i=0,1,2$) and the secondary radiative decay, $2^3P_{J_i}\,nlj \rightarrow 1^1S_0\,nlj$, would result in satellites to the principal $2^3P_{J_i} \rightarrow 1^1S_0$ lines. This process of radiative cascades via AI states may have interesting consequences for plasma diagnostics involving satellite and principal line spectra. At each step in the cascading scheme there would be competition between AI and radiative decay and the satellite intensities would depend on cascades from higher AI states. For example, if we consider the line ratio $(2^3P_2 \rightarrow 1^1S_0)/(2^3P_1 \rightarrow 1^1S_0)$, usually labeled x/y, then although both lines are enhanced through unresolved satellites populated partly from cascades, the y satellites have higher radiative probability (versus AI) than the x satellites and the y line would be *more* enhanced than the x. The observed ratio x/y would therefore be smaller than if the cascade mechanism described above were not taken into account. This may, in part, explain some anomalous observations of the x/y ratio in highly ionized He-like ions.[9]

In Figs. 2(a), 2(b), and 2(c) we examine the $\Delta n=0$ for-

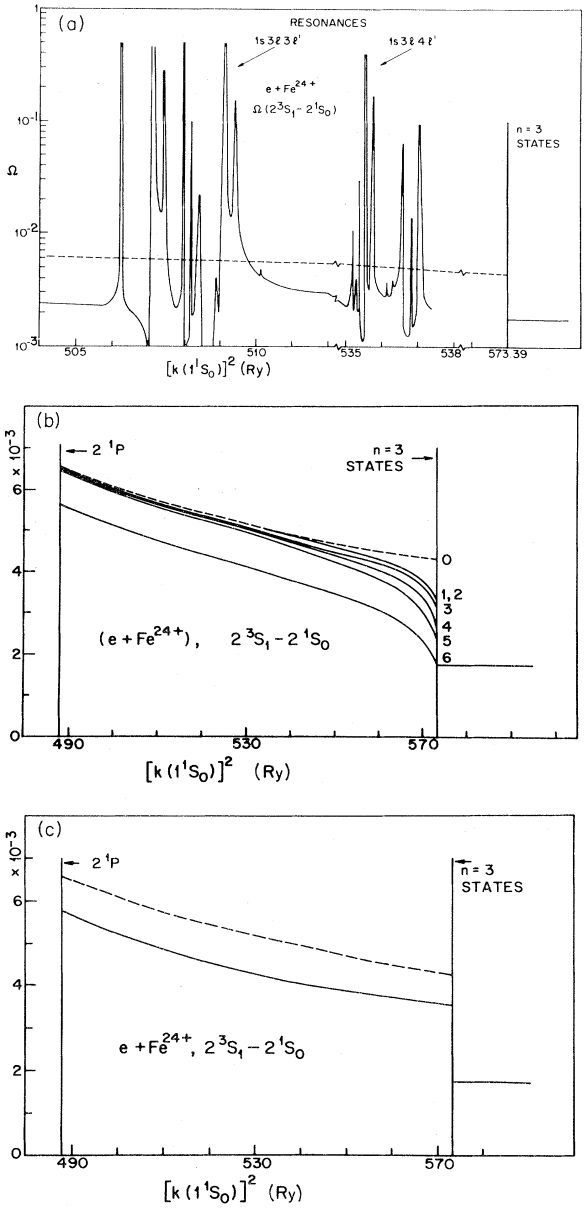

FIG. 2. Collision strength for the transition 2^3S_1-2^1S_0: (a), (b), and (c) are as in Fig. 1.

bidden transition 2^3S_1-2^1S_0 in the same manner as the 1^1S_0-2^3S_1 transition. Figure 2(a) shows a similar resonance structure and resulting enhancement of more than a factor of 2 over the nonresonant collision strength. However, in Figs. 2(b) and 2(c) we see a significant difference from the earlier case. In Fig. 2(a), the line marked 6 (corresponding to the state 3^1P_1) is much lower than the rest. This is because much of the resonance enhancement in the transition 2^3S_1-2^1S_0 arises from the series $3^1P_1\,nlj$, which upon allowed to undergo radiative decay does so with a high probability directly to the ground state. Therefore, there is a large drop in the DER contribution even in the energy range just above the excitation threshold [in contrast with Fig. 1(b)]. Figure 2(c) gives, as before, the contribution due to DER directly to ground state and it is much larger than that for the transition 1^1S_0-2^3S_1 shown in Fig. 1(c). The large AI enhancement from the $3^1P_1\,nlj$ series is due to strong coupling with the final continuum $2^1S_0\,k^2l$. We consider the problem in some more detail. The various modes of excitation and deexcitation for the two transitions may be indicated as follows:

$$\text{(i) } 1^1S_0\text{-}2^3S_1\text{: } 1^1S_0\,k_1^2l \rightarrow \begin{Bmatrix} 3^3P_1\,nl \\ 3^1P_1\,nl \end{Bmatrix} \begin{matrix} \text{AI} \rightarrow 2^3S_1\,k_2^2l \\ \text{DER} \rightarrow 1^1S_0\,nl \end{matrix}$$

$$\text{(ii) } 2^3S_1\text{-}2^1S_0\text{: } 2^3S_1\,k_2^2l \rightarrow \begin{Bmatrix} 3^3P_1\,nl \\ 3^1P_1\,nl \end{Bmatrix} \begin{matrix} \text{DER} \rightarrow 1^1S_0\,nl \\ \text{AI} \rightarrow 2^1S_0\,k_4^2l \end{matrix}$$

(the subscript i in k_i^2 refers to the term index). A measure of the strength of coupling between two types of resonance states and the final-state continuum is the ratio

$$f(2^3S_1 \rightarrow 3^3P_1)/f(2^3S_1 \rightarrow 3^1P_1) \cong 11.5$$

for (i), and

$$f(2^1S_0 \rightarrow 3^3P_1)/f(2^1S_0 \rightarrow 3^1P_1) \cong 0.09$$

for (ii). The f values are from Table II of paper I. There is a much stronger coupling between the $2^3S_1\,k_2^2l$ continuum and the resonance states $3^3P_1\,nl$ than with the $3^1P_1\,nl$. Hence, most of the resonance enhancement in the transition 1^1S_0-2^3S_1 comes from $3^3P_1\,nl$. PNH have pointed out that, considering the resonance converging on to the $n=2$ complex, the dominant contribution is from the $2^3P\,nl$ and a much smaller one from the $2^1P\,nl$—the same argument applies here. In the transition 2^3S_1-2^2S_0, however, the situation is reversed and it is the $3^1P_1\,nl$ series that provides the dominant resonance contribution. But the total DER effect on the cross sections depends on the radiative probabilities $A(3^3P_1 \rightarrow 1^1S_0)$ and $A(3^1P_1 \rightarrow 1^1S_0)$ and since the former is about an order-of-magnitude smaller than the latter, the DER reduction in AI is much larger for the 2^3S_1-2^1S_0 transition than for the 1^1S_0-2^3S_1.

Figure 3 is a plot of $\Omega(1^1S_0$-$2^3P_1)$ with similar structure as the other two collision strengths [note that the ordinates in Figs. 1(a), 2(a), and 3 are on a log scale and that the resonances go up to 2 or 3 orders-of-magnitude above the background]. However, here the dashed line (Gailitis average) joins almost exactly with the solid line at the $n=3$ threshold indicating that there is no overall enhancement in the effective collision strengths. In IC, 1^1S_0-2^3P_1 is an allowed transition (see paper I) with strong background scattering potential (mainly dipole) and, therefore, the resonance contribution relative to the nonresonant part is not significant. In the figures showing resonance structures there may be some discrepancy in the detailed features or the magnitude since we have employed different approximations to analyze the two groups of resonances. However, the difference should be slight as is evident by inspection and by the distribution about the averaged collision strengths.

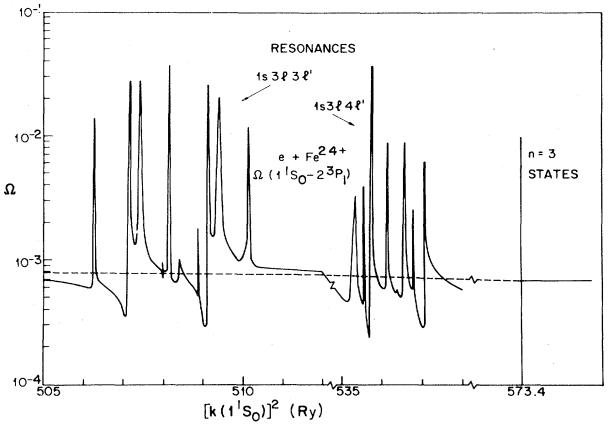

FIG. 3. Collision strength for the transition 1^1S_0-2^3P_1 showing detailed resonance structure and the averaged values (nearly equal to the background collision strength, i.e., no significance resonance contribution).

In order to obtain a quantitative and qualitative assessment of the effect of DER as the ion charge increases, we plot in Fig. 4 $\Omega(1^1S_0$-$2^3S_1)$ for Mo^{40+}. As the resonance features and the AI enhancement remain approximately the same as for Fe^{24+}, only the averaged collision strengths are considered. It is found that the area enclosed between the dashed line (AI average $\langle\Omega\rangle$) and the solid line (AI average including DER, $\langle\Omega\rangle_d$) is approximately 30% of the area between the $\langle\Omega\rangle$ and the background collision strength extrapolated to threshold energy. As mentioned earlier, for Fe^{24+} the same figure is slightly

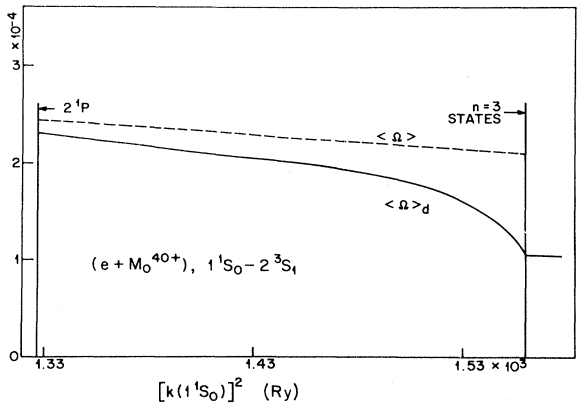

FIG. 4. Resonance averaged collision strength $\langle\Omega(1^1S_0$-$2^3S_1)\rangle$ for Mo^{40+} (dashed line) and including the effect of DER, $\langle\Omega\rangle_d$ (solid line).

TABLE III. Intermediate-coupling autoionization and dielectronic recombination contributions to collision strengths for Fe^{24+}. The notation 3.29(−4) is a shorthand for 3.29×10^{-4}.

Transition	Ω^{LS}	Ω^{IC}	$\langle\Omega\rangle^{(IC+AI)}$	$\langle\Omega\rangle^{(IC+AI+DER)}$	Net resonance enhancement with respect to Ω^{IC} (%)
1^1S_0-2^3S_1	3.29(−4)	3.20(−4)	6.38(−4)	6.18(−4)	93.1
1^1S_0-2^3P_0	2.14(−4)	2.15(−4)	2.75(−4)	2.71(−4)	26.0
1^1S_0-2^3P_1	6.42(−4)	7.62−4)	8.24(−4)	8.14(−4)	6.8
1^1S_0-2^3P_2	1.07(−3)	1.08(−3)	1.37(−3)	1.36(−3)	26.0
1^1S_0-2^1S_0	6.59(−4)	6.59(−4)	8.39(−4)	8.08(−4)	22.6
1^1S_0-2^1P_1	2.20(−3)	2.06(−3)	2.65(−3)	2.62(−3)	27.2
2^3S_1-2^1S_0	2.76(−3)	2.77(−3)	6.27(−3)	5.31(−3)	91.7
2^3S_1-2^1P_1	4.69(−3)	2.04(−2)	2.41(−2)	2.37(−2)	16.2
2^3P_0-2^3P_1		8.36(−3)	1.11(−2)	1.10(−2)	31.6
2^3P_0-2^3P_2		8.74(−3)	1.01(−2)	9.91(−3)	13.4
2^3P_0-2^1S_0	5.16(−4)	5.14(−4)	8.52(−4)	8.13(−3)	58.2
2^3P_0-2^1P_1	3.74(−3)	4.04(−3)	4.74(−3)	4.56(−3)	12.9
2^3P_1-2^3P_2		2.94(−2)	3.66(−2)	3.59(−2)	22.1
2^3P_1-2^1P_1	1.12(−2)	1.39(−2)	1.42(−2)	1.39(−2)	0.0
2^3P_2-2^1S_0	2.58(−3)	2.57(−3)	4.26(−3)	4.08(−3)	58.8
2^3P_2-2^1P_1	1.87(−2)	1.98(−2)	2.37(−2)	2.27(−2)	14.6

greater than 10%. Therefore, while the AI enhancement for Fe^{24+} and Mo^{40+} is about the same, a factor of 2, the DER reduction in Mo^{40+} is about 3 times that in FE^{24+}, reflecting the higher radiative decay probabilities of the resonance states.

Finally, in Table III we bring together some results from paper I and the present one to illustrate the particular effect under consideration in the present study. All transitions up to and including the $n=2$ levels in Fe^{24+} are given (except for those optically allowed transitions where the partial waves higher than $l=4$ make a significant contribution). Calculations are carried out at an energy some where above the 2^1P_1 level. The column $\langle\Omega\rangle^{(IC+AI+DER)}$ gives the net effective collision strengths and the last column shows the percentage enhancement of these values over the background collision strengths in IC (Ω^{IC}). Clearly, resonance enhancement is quite significant— nearly a factor of 2 for 1^1S_0-2^3S_1 and 2^3S_1-2^1S_0. For most transitions the enhancement continues until fairly close to the $n=3$ threshold where all resonances must decay radiatively and the effective cross section falls down to the background level. The transition 2^3S_1-2^1P_1 shows a 16% resonance effect but this is quite different from the effect in *LS* coupling discussed by PNH where, since the transition is forbidden, there are several factors to consider (this transition is also discussed by Clark *et al.*[10]).

Table IV compares the various collision strengths for a few transitions in Mo^{40+}, again computed at an energy just above the 2^1P_1 level (although it is not exactly the same scaled energy as for Fe^{24+} in Table III). The net resonance enhancement for most transitions is less than in Fe^{24+} due to *increase* in the negative DER contribution. For example, the percentage figure for 2^3S_1-1^1S_0 is 67.3 compared with 91.7 for Fe^{24+}. As discussed above, the DER process for a given transition depends on the radiative probability and the magnitude of coupling between the initial and final states and the particular resonance states. Hence, the resulting decrease in AI due to DER, with Z, is not uniform for all transitions. $\Omega(1^1S_0$-$2^3S_1)$ in

TABLE IV. Intermediate-coupling autoionization and dielectronic recombination contributions to collision strengths for Mo^{40+}.

Transition	Ω^{LS}	Ω^{IC}	$\langle\Omega\rangle^{(IC+AI)}$	$\langle\Omega\rangle^{(IC+AI+DER)}$	Net resonance enhancement with respect to Ω^{IC} (%)
1^1S_0-2^3S_1	1.30(−4)	1.21(−4)	2.44(−4)	2.30(−4)	90.1
1^1S_0-2^3P_0	8.32(−5)	8.50(−4)	1.01(−4)	9.64(−4)	13.4
1^1S_0-2^3P_2	4.16(−4)	4.24(−4)	5.06(−4)	4.84(−4)	14.2
1^1S_0-2^1S_0	2.62(−4)	2.62(−4)	3.32(−4)	3.20(−4)	22.1
2^3S_1-2^1S_0	1.06(−3)	1.07(−3)	2.04(−3)	1.79(−3)	67.3
2^3P_0-2^3P_1		3.01(−3)	3.58(−3)	3.34(−3)	11.0
2^3P_0-2^1S_0	1.96(−4)	1.93(−4)	2.61(−4)	2.31(−4)	19.7
2^3P_1-2^3P_2		1.06(−2)	1.23(−2)	1.14(−2)	7.5
2^3P_2-2^1S_0	9.78(−4)	9.65(−4)	1.30(−3)	1.17(−3)	21.2

Mo^{40+} shows only a marginal decrease compared with Fe^{24+}.

It is of some interest to see exactly how the ratio of AI versus radiation probabilities behaves with energy from near the excitation threshold to the threshold of convergence for a given ion and a specific symmetry. In Table V we calculate this ratio at three energies between the $n=2$ and the $n=3$ complexes. The symmetry under consideration is $J=2.5$, odd parity, whose channel list is given in Table III of paper I. The ratio is calculated for a few closed channels, one for each $n=3$ fine-structure state, and designated as $S_iL_iJ_il_i(Ks)J\pi$. The K value corresponding to these channels is 2, except for the 3^1S_0, where it is 3. The values of the ratio given indicate that autoionization dominates radiation at the energy close to the excitation threshold for all channels, but is much less than unity near the convergence threshold. The 3^1P_1l channels, as expected, have the highest radiative probabilities.

One of the main aims of the present work is to compute accurate collision strengths in order to obtain rate coefficients for applications in plasma diagnostics. Our earlier work (PNH) employing simpler approximations than in the present study, enabled us to compute rate coefficients for a number of ions (Pradhan *et al.*[11]) including, for the first time, resonance structures in collision strengths. Calculations were recently carried out by Kingston and Tayal[12] for one of the ions, O VII, in an elaborate eleven-state close-coupling approximation. Their results for the rate coefficients of the two transitions considered 1^1S-2^3S and 1^1S-2^3p agree fairly well with those of Pradhan *et al.* (10—20%), confirming the fact that resonances play an important role in scattering with He-like ions for some transitions. The resonance enhancement in the transition 1^1S-2^3S in O VII was found to be about 85% at 10^6 K. From the present work we see that the resonance effect remains large even for highly charged ions and even after the effect of radiation is accounted for. In Table VI we give the rate coefficients for 1^1S_0-2^3S_1 in Fe^{24+} and Mo^{40+} to illustrate this point. Although there is little difference between the rate coefficients with and without DER for Fe^{24+}, we should expect the difference to be significant as the ion charge increases further. Comparing the rate coefficient as a Z-scaled temperature, $T/Z^2=2.84\times10^4$, corresponding to 2.0×10^7 K for Fe^{24+} and 5.0×10^7 K for Mo^{40+}, we find that the decrease due to DER is 9% and 19%, respectively [the percentage figure is $(q_A-q_D)\times100/q_B$]. The overall resonance enhancement in Mo^{40+} is less than that in Fe^{24+}, mainly because the temperatures are higher and therefore there is a larger contribution to the rate coefficient from the nonresonant region above the $n=3$ levels (the Maxwellian distribution falls off much more slowly). Bely-Dubau *et al.*[13] have computed the rate coefficients for a few transitions in Fe^{24+} using a nonresonant Dw approximation. Their value at 3×10^7 K for $q(1^1S_0$-$2^3S_1)$ is 3.15×10^{-14}, which compares well with our background value q_B in Table VI.

TABLE V. Ratio of autoionization vs radiation effects: Fe^{24+}, $J=2.5$, odd π. ($A_a=\sum_k|\chi_{nk}|^2$ and $AR(n)=2\pi\nu^3/z^2\sum_b\Gamma_{nb}$ [see Eq. (11)]).

Closed channel (n)[a]	$k_1^2=$	$A_a/AR(n)$ 495.0	525.0	570.0
3^3S_1p (18)		1.06(2)	4.64(1)	5.76(−1)
3^3P_0d (21)		6.81(0)	7.58(−1)	1.05(−2)
3^3P_1d (22)		2.62(0)	8.69(−1)	1.94(−2)
3^3P_2s (25)		3.17(0)	1.04(0)	2.02(−2)
3^1S_0f (30)		6.11(0)	2.69(0)	1.73(−1)
3^1P_1d (31)		1.85(0)	8.14(−1)	10.5(−2)

[a]The index corresponds to Table III of paper I. Threshold of convergence, $E(n=3)$, is 573.39 Ry.

V. CONCLUSION

Some of the conclusions drawn from the present study should be generally valid for electron scattering from highly charged ions; others may be particular to the helium isoelectronic sequence. A summary of the main points is given below.

(i) All three effects, IC, AI, and DER, are important in electron excitation of very highly ionized atoms.

(ii) AI enhancement, for a given transition, approaches a nearly constant factor in the limit of high Z.

(iii) DER reduction in AI depends on (a) the magnitude of the contribution of a particular resonance series and (b) the total radiative decay probability (i.e., the sum over all possible core transitions). Condition (a) reflects the strength of coupling between the resonance states and the initial and final states in the transition.

(iv) Final stabilization in DER may take place in a number of steps resulting in radiative cascade contributions to satellite levels (these contributions may be estimated using the methods described).

(v) Although the forbidden core transitions ($E2$, $2E1$, $M1$, and $M2$ type) scale much more rapidly with Z than the allowed ones (Z^8 vs Z^4; $M1$ transition, 1^1S_0-2^3S_1, scales as Z^{10}), they are not expected to contribute significantly to DER until about $Z>50$. Experimentally, one should then be able to observe the forbidden dielectronic

TABLE VI. Rate coefficients $q(1^1S_0$-$2^3S_1)$. q_B, with nonresonant, background collision strengths; q_A, with AI resonances (no DER); q_D, including DER. These are the final net rate coefficients. Rate coefficients are given in units of $cm^3\,sec^{-1}$. The last temperature for each ion is close to the temperature of maximum resonance line emission (from the $2^1P_1\rightarrow1^1S_0$ transition).

Ion	T(K)	q_B	q_A	q_D
Fe^{24+}	1×10^7	3.61(−16)	6.44(−16)	6.05(−16)
	2×10^7	1.10(−14)	1.73(−14)	1.63(−14)
	3×10^7	3.35(−14)	4.81(−14)	4.56(−14)
	5×10^7	5.83(−14)	7.76(−14)	7.43(−14)
Mo^{40+}	5×10^7	2.17(−15)	3.51(−15)	3.10(−15)
	8×10^7	7.12(−15)	1.05(−14)	9.42(−15)
	1×10^8	1.02(−14)	1.45(−14)	1.31(−14)
	3×10^8	1.65(−14)	2.11(−14)	1.95(−14)

satellite spectra.

A few general purpose techniques have been discussed in the present work and should prove to be useful in further calculations on highly ionized systems. Work in progress includes (a) rate coefficients for all transitions, up to and including the $n=3$ levels, for Ca^{18+}, Fe^{24+}, Se^{32+}, and Mo^{40+}, (b) comparison of detailed autoionization profiles in the DW and CC approximations, (c) dielectronic satellite intensities for temperature diagnostics, and (d) DER cross sections and rate coefficients employing the same methods as described in this work. Both the electron excitation and the DER rates could be obtained in a unified formulation, thus providing a measure of self-consistency and better accuracy in practical applications.

ACKNOWLEDGMENTS

This work was supported by the Natural Sciences and Engineering Research Council of Canada.

---

*Present address: Joint Institute for Laboratory Astrophysics, University of Colorado and National Bureau of Standards, Boulder, Colorado 80309.

[1]M. J. Seaton, J. Phys. B 2, 5 (1969).

[2]M. Gailitis, Zh. Eksp. Teor. Fiz. 44, 1974 (1963) [Sov. Phys.—JETP 17, 1328 (1963)].

[3]L. P. Presnyakov and A. M. Urnov, J. Phys. B 8, 1280 (1975).

[4]A. K. Pradhan, Phys. Rev. Lett. 47, 79 (1981).

[5]H. E. Saraph, Comput. Phys. Commun. 15, 247 (1978); 3, 256 (1972).

[6]A. K. Pradhan (unpublished).

[7]W. Eissner and M. J. Seaton, J. Phys. B 7, 2533 (1974).

[8]P. de A. P. Martins and M. J. Seaton, J. Phys. B 2, 333 (1969).

[9]E. Källne, J. Källne, and A. K. Pradhan, Phys. Rev. A 27, 1476 (1983).

[10]R. E. H. Clark, N. H. Magee, Jr., J. B. Mann, and A. L. Merts, Astrophys. J. 254, 412 (1982).

[11]A. K. Pradhan, D. W. Norcross, and D. G. Hummer, Astrophys. J. 246, 1031 (1981).

[12]A. E. Kingston and S. S. Tayal, J. Phys. B 16, L53 (1983).

[13]F. Bely-Dubau, J. Dubau, P. Faucher, and A. H. Gabriel, Mon. Not. R. Astron. Soc. 198, 239 (1982).